

LIFTING THE DUSTY VEIL WITH NEAR- AND MID-INFRARED PHOTOMETRY: III. TWO-DIMENSIONAL EXTINCTION MAPS OF THE GALACTIC MIDPLANE USING THE RAYLEIGH-JEANS COLOR EXCESS METHOD

DAVID L. NIDEVER, GAIL ZASOWSKI, & STEVEN R. MAJEWSKI
Department of Astronomy, University of Virginia, Charlottesville, VA 22904
Draft version November 6, 2018

ABSTRACT

We provide new, high-resolution $A(K_s)$ extinction maps of the heavily reddened Galactic midplane based on the Rayleigh-Jeans Color Excess (“RJCE”) method. RJCE determines star-by-star reddening based on a combination of near- and mid-infrared photometry. The new RJCE-generated maps have $2' \times 2'$ pixels and span some of the most severely extinguished regions of the Galaxy — those covered with *Spitzer*+IRAC imaging by the GLIMPSE-I, -II, -3D, and Vela-Carina surveys, from $256^\circ < l < 65^\circ$ and, in general, for $|b| \leq 1^\circ$ – 1.5° (extending up to $|b| \leq 4^\circ$ in the bulge). Using RJCE extinction measurements, we generate dereddened color-magnitude diagrams and, in turn, create maps based on main sequence, red clump, and red giant star tracers, each probing different distances and thereby providing coarse three-dimensional information on the relative placement of dust cloud structures. The maps generated from red giant stars, which reach to ~ 18 – 20 kpc, probe beyond most of the Milky Way extinction in most directions and provide close to a “total Galactic extinction” map — at minimum they provide high angular resolution maps of lower limits on $A(K_s)$. Because these maps are generated directly from measurements of reddening by the very dust being mapped, rather than inferred on the basis of some less direct means, they are likely the most accurate to date for charting in detail the highly patchy differential extinction in the Galactic midplane. We provide downloadable FITS files and an IDL tool for retrieving extinction values for any line of sight within our mapped regions.

Subject headings: Galaxy: structure – Galaxy: disk – reddening, dust, infrared techniques

1. INTRODUCTION

The existence of interstellar dust and its light-obscuring effects, though postulated more than a century and a half ago by Struve (1847) as one (incorrect) solution to Olber’s Paradox, was not definitively proven until Trumpler’s (1930) insightful experiment to compare distances of open clusters derived in separate extinction-dependent and extinction-independent methods. Though the amount of extinction resulting from this dust was historically often approximated with a standard accumulation by distance under an assumed plane-parallel distribution (i.e., the cosecant law; e.g., Shane & Wirtanen 1967, Peterson 1970, Noonan 1971, Sandage 1973, de Vaucouleurs, de Vaucouleurs & Corwin 1976, de Vaucouleurs & Buta 1983, Fabbri et al. 1986; but see Kron & Guetter 1973, Holmberg 1974, Knude 1996 for examples of discussions of simple variations about the basic cosecant law), it was always well-understood that the distribution of Galactic dust is in fact quite irregular.¹ Once it is appreciated that an irregular selective obscuration of a more regular distribution of stars, and not an irregular distribution of the stars themselves, is shaping the net configuration of observed starlight, then any observation of the density of — or light from — stars in the Galactic plane of the Milky Way clearly illustrates

this patchiness (e.g., Herschel’s [1785] drawings of the distribution of stars in the Milky Way, or the early photographs of the Galactic plane by Barnard et al. 1927).

For extragalactic studies, a long-standing default strategy has been simply to steer clear of the “Zone of Avoidance” at low Galactic latitudes altogether, rather than contend with assessing the amount of foreground extinction. Unfortunately, Nature is not always so accommodating with the placement of important and interesting sources, and corrections for foreground dust — generally attributable to dust in our own Milky Way — are almost always needed; even at the highest Galactic latitudes, one can encounter appreciable amounts of dust (e.g., the North Galactic Pole has $A(B)$ as high as 0.05 to 0.1 mags, depending on the reddening calibration and extinction law used; e.g., Hilditch et al. 1983, Knude 1996, Peek & Graves 2010).

Early attempts to map the variation of total line-of-sight Galactic extinction explored a number of techniques. For example, under an assumed constancy of dust-to-gas ratio, the net column density of HI, easily measured via 21-cm observations, could be converted into a dust column density (e.g., Lilley 1955, Sturch 1969, Savage & Jenkins 1972, Knapp & Kerr 1974, Burstein & Heiles 1982). Under the assumption of a homogeneous spatial distribution of galaxies, the counts of galaxies to a given magnitude limit were also used to infer the degree of extinction along a line of sight (Burstein & Heiles 1978, 1982). Similarly, the assumption of spatial constancy of the *stellar* distribution (at least on relatively small angular scales) has been employed to derive extinction using star counts — comparing stellar densities across a clearly

dln5q, gz2n, srm4n@virginia.edu

¹ Even relatively recently, Knude (1996) went through great pains to determine whether the cosecant law can at least provide a reasonable approximation in the North Galactic polar cap and concluded that only a piecewise application of the cosecant law with varying coefficients can work, and only in certain ranges of Galactic latitude and longitude.

extinguished region (often on the edges of a dark cloud) to those in nearby “control” regions (e.g., Wolf 1923, Bok 1956, Froebrich et al. 2005).

Directly *measuring* the effects of dust via such affected tracers is the most reliable method to map the Galactic extinction. Extracting the reddening and extinction effects of foreground dust from the intrinsic spectral energy distributions (SEDs) of observed sources has traditionally required direct, detailed spectroscopic information of each source to classify it explicitly and thereby infer its intrinsic properties independent of observed colors — quite a demanding prospect in most situations. In recent decades, a large body of work has amassed that attempts to determine the total amount of extinction foreground to heavily-reddened sources by *photometric* means; under the assumption of a homogeneous color distribution of either stars or galaxies (or particular classes of either), deviations from the mean observed colors are attributed to interstellar reddening. The decreased temperature dependencies of infrared (IR) colors, combined with the decreased extinction effects at IR wavelengths, has led to the wide adoption of IR and optical-IR color excesses as high-quality gauges of interstellar reddening, especially in highly extinguished regions (since e.g., Jones et al. 1980, 1984, Smith 1987). Lada et al. (1994) introduced a powerful and efficient method of extinction mapping with the NICE (Near Infrared Color Excess) technique, which applies elements of both IR excess measurements and star-counting techniques to large sets of IR photometry; this method has undergone significant evolution (NICER, Lombardi & Alves 2001; V-NICE, Gosling et al. 2009; NICEST, Lombardi 2009) and has been applied to a series of dense clouds and dark nebulae (e.g., Alves et al. 1998, Lada et al. 2009, Lombardi et al. 2010). The color excess method has also been applied to galaxy colors (e.g., Peek & Graves 2010), though galaxy ensembles are obviously best-suited to gauging *total* line-of-sight Galactic reddening. Greater accuracy may be attained through use of objects with well-defined (and limited ranges of) colors like RR Lyrae stars, globular clusters, or red clump stars. Another method advocated by Burstein and collaborators (Burstein et al. 1988, Faber et al. 1989) is based on the observation that the integrated spectra of the stellar populations of giant elliptical galaxies are strikingly uniform, so that the intrinsic $(B - V)_0$ colors of these systems can be inferred on the basis of the spectroscopic measurement of their Mg_2 line index.

Early investigations into the consistency of extinction derived with these various methods generally led to disappointing results, with no simple relationships found amongst the different dust proxies (Heiles 1976). Partly this is because of the failure of the very assumptions on which each method is based — e.g., the high “noise” in galaxy counts due to large scale structure, or variations in the dust-to-gas ratio (Seki 1973, Jenkins & Savage 1974, Bohlin 1975, Savage et al. 1977, Burstein & Heiles 1978, Fong et al. 1987, Burstein 2003).

Currently the most commonly used large-scale reddening maps are those by Schlegel, Finkbeiner & Davis (1998, “SFD” hereafter), which have been derived from $100\mu\text{m}$ emission maps using the COBE/DIRBE and IRAS/ISSA data. These maps have proven reliable for differential line-of-sight reddening in low extinction regions, albeit with some uncertainties in zero-points (see

discussion by Burstein 2003). Unfortunately, these maps have a resolution of only $\sim 6'$, which is particularly problematical where the reddening varies dramatically on much smaller angular scales. In addition, a number of studies have shown that the SFD maps overestimate the extinction at low latitudes by as much as 50% in $A(V)$ (Stanek 1998a,b, Arce & Goodman 1999a, Chen et al. 1999, Ivans et al. 1999, von Braun & Mateo 2001, Choloniewski & Valentijn 2003, Rocha-Pinto et al. 2004, Dutra et al. 2003a,b, Cambrésy et al. 2005, Amôres & Lépine 2005, 2007, Yasuda et al. 2007, Peek & Graves 2010). A physical reason for the complications of the SFD maps at low latitudes is explored in the analysis in Paper I — namely that far-infrared-*emitting* dust, which provides the basis of the SFD extinction maps, is simply not a good proxy for the dust causing *extinction* at shorter wavelengths. Comparison to other extinction tracers reveals that many of the SFD “high extinction” knots actually trace supernova remnant or star-forming environments, and a number of cold, dense clouds can be identified in extinction that lack the far-IR emission actually traced by the SFD maps.

Thus, the midplane extinction in the Milky Way is far from being unambiguously mapped, and for studies of the Milky Way itself, the patchy intermingling of dust and stars remains a particularly troublesome obstacle. Both photometric and spectroscopic parallax determinations must include an accurate assessment of the extinction *foreground* to a star to gauge its distance. While studies of specific dark clouds using stellar IR color excess methods (particularly the extensive NICE family of techniques) have achieved remarkable success at mapping extinction, reliable assessments of extinction foreground to stars and astronomical sources *not* associated with these dark clouds have proven more elusive.

Now, more accurate measurements of individual stellar extinction levels, including full three-dimensional spatial distribution information, is becoming possible through combined near- and mid-IR observations of the Rayleigh-Jeans flux distributions of stars (Majewski et al. 2011, Paper I hereafter); because the long wavelength SEDs of normal stars have approximately the same shape (i.e., colors) on their Rayleigh-Jeans tails, the *observed* Rayleigh-Jeans colors contain information on the foreground reddening to a star explicitly. We show in Paper I that this Rayleigh-Jeans Color Excess (RJCE) method is superior to the SFD method for mapping the extinction by midplane dust and is an improvement over the other IR color-excess methods due to the improved homogeneity of RJCE’s adopted color indices. An additional advantage of the RJCE method over its predecessors is that the former cleanly separates reddening from intrinsic stellar colors and preserves the latter for use in the identification of stellar types (e.g., main sequence versus red clump versus red giant); thus, we can use the RJCE method to fairly reliably isolate the most distant stellar proxies (i.e., red giants) to create the best assessment of the total reddening along a given line of sight. Alternatively, one can isolate a rather reliable standard candle (in the form of red clump stars) to bring greater accuracy to distance estimates. In combination, stellar types of different intrinsic luminosity can yield the distance distribution of the dust along the line of sight.

In this contribution to the present series of papers on

the RJCE method, we make new, two-dimensional extinction maps of the Galactic midplane across the entire Galactic Legacy Infrared Mid-Plane Survey Extraordinaire (GLIMPSE-I; Benjamin et al. 2003; GLIMPSE-II/-3D Churchwell et al. 2009), and Vela-Carina (*Spitzer* PID 40791) IRAC survey areas. Section 2 summarizes how the maps were created; the reader is directed to Paper I for a fuller description and analysis of the RJCE method and its application to different color index combinations and different stellar types. In Section 3 we present a full atlas of these maps based on use of main sequence, red clump, and red giant tracers, and in Section 4 we alert the reader to various caveats for using the maps. Electronic versions of these maps have been made publicly available, and we describe how to access them in Section 5.

2. CREATION OF THE MAPS

2.1. Summary of the RJCE Method

IR imaging, like that in 2MASS (Skrutskie et al. 2006) and UKIDSS (Lucas et al. 2008), can more efficiently penetrate the obscuration in the dusty midplane and Galactic Center than observing at shorter wavelengths, and much work has been done using IR observations of low-latitude stars as probes of Galactic structure and the interstellar medium (ISM) there. Measuring “color excesses” is one common use of this NIR photometry — comparing the observed colors of a star (or the average of a group of stars) to the expected intrinsic colors to determine the amount of line-of-sight reddening, which can then be converted into an extinction under an assumed extinction law. Figure 1 in Paper I demonstrates some of the primary complications when this method is applied to broadband NIR colors in isolation. First, the spread in intrinsic NIR color is significant: A, F, G, and K stars span about a magnitude in $(J - H)_0$ and $(J - K_s)_0$ and almost half of a magnitude in $(H - K_s)_0$. In addition, the NIR reddening vector very closely parallels the intrinsic stellar locus, leading to high degeneracy in derived reddening estimates based on observed stellar colors.

Both of these critical problems are greatly ameliorated by using longer-wavelength, longer-baseline colors including MIR photometry from, e.g., the *Spitzer Space Telescope’s* IRAC instrument. These longer-wavelength filters sample the Rayleigh-Jeans tail of a normal star’s SED; the slope of this tail (and thus the colors measured from it) has very little dependence on stellar temperature, so the intrinsic variation in MIR and NIR-MIR colors is significantly smaller than in NIR colors. For example, the A–K stars mentioned earlier differ by only ~ 0.1 mag in $(H - [4.5\mu])_0$. Furthermore, the reddening vector in these colors is very nearly perpendicular to the stellar RGB locus², facilitating more accurate estimates of the stellar reddening. The RJCE method takes advantage of these NIR-MIR color properties to produce reliable estimates of the line-of-sight reddening to each individual star. Analysis of many factors, including intrinsic color variation and typical photometric quality (see Paper I), has led us to adopt $(H - [4.5\mu])$ as the best single NIR-MIR color for stellar dereddening.

² It is true that the reddening vector more closely parallels the locus of cool main-sequence stars; however, these are very sparse in the 2MASS and GLIMPSE surveys

Also shown in Paper I are comparisons of RJCE-derived extinction maps to those of SFD as well as to maps of ^{13}CO emission, $8\mu\text{m}$ dust and PAH emission, and NIR star counts. The RJCE maps bear a striking structural similarity to the ^{13}CO and star count maps, both expected to be good tracers of cold, dense extinction regions, while the SFD maps more closely resemble the $[8.0\mu]$ images.

Moreover, the RJCE method *directly* measures the reddening on a star-by-star basis, and is therefore superior to methods that use proxies to calculate extinction (e.g., dust emission, HI, or galaxy counts). The RJCE method relies only on the availability of stars, which are, fortunately, very abundant in those parts of the Galaxy where the effects of dust are strongest.

2.2. Defining the Stellar Samples

Arguably, the RJCE method’s most powerful and unique feature is the ability to recover a star’s approximate stellar type after the reddening has been estimated. The strong temperature dependence of the *corrected* NIR colors (especially those involving *J*-band) allows us to derive an approximate photometric temperature (hence spectral type and, based on the apparent magnitude, the luminosity class as well³). For the initial publicly-available maps presented here, we have used this powerful feature to split the 2MASS+*Spitzer* stellar sample into three subsamples: main sequence (MS) dwarfs, which are dominant for $0.0 \leq (J - K_s)_0 \leq 0.5$, red clump (RC) giants for $0.55 \leq (J - K_s)_0 \leq 0.85$, and red giant branch (RGB) giants for $0.85 < (J - K_s)_0 \leq 1.4$, where $(J - K_s)_0$ for each star is calculated using the RJCE method described in Section 2.1 and Paper I. See Figure 1 for an example of a corrected color-magnitude diagram (CMD) and the rationale for the adopted stellar color divisions. Each of these stellar subsamples probes a different range of heliocentric distance (see §4.2 and Figure 5), so maps using each tracer, taken together, provide coarse *three-dimensional* information about the midplane dust distribution, based solely on which of the actual stellar tracers are being reddened.

3. EXTINCTION MAPS OF THE MILKY WAY MIDPLANE

Figure 3 contains the “Version 1” RJCE extinction maps, in units of $A(K_s)$, over $\sim 170^\circ$ of longitude in the Galactic midplane. For $|l| \leq 65^\circ$, the latitude range is centered on the Galactic equator (and includes $|b| \leq 1^\circ$ for most longitudes but up to $|b| \leq 4^\circ$ in the bulge). In the longitude range covered by the Vela-Carina survey ($295^\circ \leq l \leq 255^\circ$), the map center varies between $b = +0.5^\circ$ and $b = -0.5^\circ$, but the latitude coverage is consistently 2° tall.

The basic procedure used to make the maps is as follows: Using the reliable band-merged 2MASS+IRAC Catalog⁴, we selected stars having detections and photometric errors < 0.2 mag in all four of the *J*, *H*, *K_s* and

³ There is certainly dwarf/giant degeneracy at redder NIR colors, but Galactic stellar population models (e.g., TRILEGAL; Girardi et al. 2005) guide us as to which magnitudes, for a given color, we may expect a low fraction of late-type dwarf contaminants. Fortunately, these models show that late-type dwarfs are in any case very rare in the 2MASS+GLIMPSE catalog.

⁴ http://irsa.ipac.caltech.edu/data/SPITZER/GLIMPSE/doc/glimpse1_dataproduct_v2.0.pdf

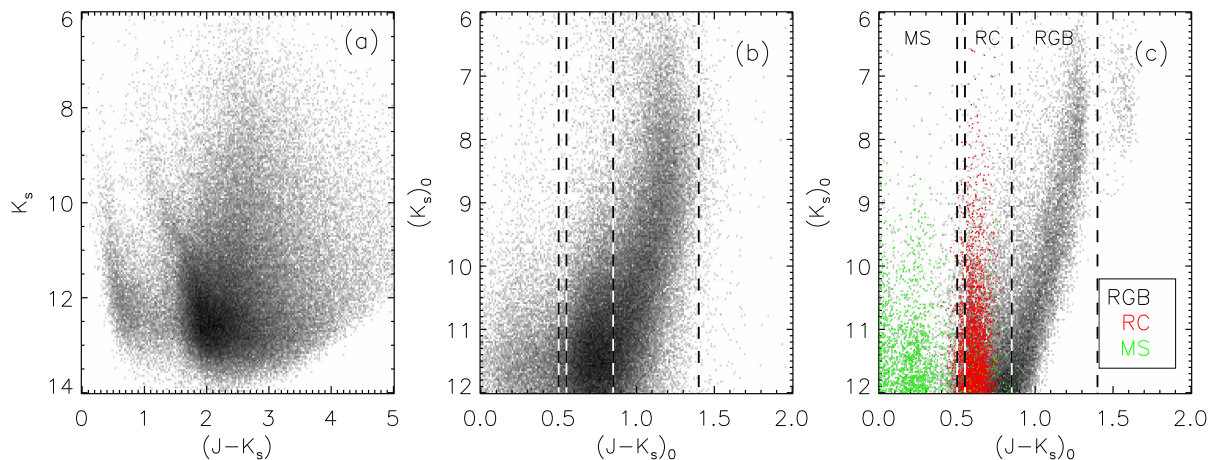


FIG. 1.— Three color-magnitude diagrams (CMDs) of a 4 deg^2 field at $(l, b) = (42.0^\circ, 0^\circ)$ for all sources with magnitude errors less than 0.5 mag in the three 2MASS and four *Spitzer*-IRAC bands. Sources are binned in bins of 0.025 in $J - K_s$ and 0.04 in K_s . (a) The raw 2MASS data. (b) The RJCE-corrected CMD. (c) An extinction-free model of the same field from TRILEGAL (Girardi et al. 2005) with photometric errors; color-coded to highlight the different stellar populations (MS—main sequence, RC—red clump, and RGB—red giant branch). The vertical dashed lines in (b) and (c) indicate the color divisions between MS, RC and RGB stars.

$[4.5\mu]$ bands. The extinction was calculated for each star separately, using

$$A(K_s) = 0.918 \times (H - [4.5\mu] - 0.08) \quad (1)$$

from Paper I. Each star was dereddened and classified as MS, RC, or RGB using the RJCE method and the stellar color bins described in Section 2. Each of these three subsamples was binned separately into a spatial map with $2'$ resolution, and two extinction maps were created for each subsample (for a total of six distinct maps) using the median and 90th percentile values of $A(K_s)$ measured within each spatial pixel. Similar maps were created for the larger sample of all stars, with no color cuts. All of these extinction maps were Gaussian smoothed (FWHM= $1.4'$) to reduce noise. Not only do the 90th percentile maps represent the majority of the extinction affecting each stellar subsample, they are also the least likely to be biased by contaminants from, e.g., foreground cool dwarfs (in the case of the RGB maps) or photometric errors. All extinction values are given in magnitudes of $A(K_s)$. We also provide star count and $A(K_s)$ dispersion (not to be confused with the uncertainty) maps for each subsample. Pixels with less than two stars in them are set to white in the $A(K_s)$ quick-look images (black in the starcount quick-look images) and have a value of 999999.0 in the queryable FITS tables.

Finally, we also include “lower limit total extinction” maps produced using only the IRAC $[3.6\mu]$ and $[4.5\mu]$ bands; these are 90th percentile extinction maps made using *all* stars with detections and photometric errors $< 0.5 \text{ mag}$ in both of these bands (see Section 4.1). To derive extinctions from $([3.6\mu] - [4.5\mu])$ we use,

$$A(K_s) = 9.188 \times ([3.6\mu] - [4.5\mu] + 0.235), \quad (2)$$

which was found by linear fitting the $E(H - [4.5\mu])$ -derived $A(K_s)$ values and the $([3.6\mu] - [4.5\mu])$ colors for all stars in the longitude range $20^\circ \leq l \leq 30^\circ$ and photometric errors in H, $[3.6\mu]$, and $[4.5\mu]$ less than 0.07 mag (see Fig. 2). The intrinsic scatter and photometric errors in $([3.6\mu] - [4.5\mu])$ are generally higher than for

$(H - [4.5\mu])$, and, therefore, the derived extinctions are generally less reliable and mainly useful for high extinction regions (where the $[H - 4.5\mu]$ maps often drop out). Including the $([3.6\mu] - [4.5\mu])$ extinction maps, there are a total of 18 maps in the downloadable FITS files, as listed in Table 1. Examples of the extinction maps are also shown in Figure 3.

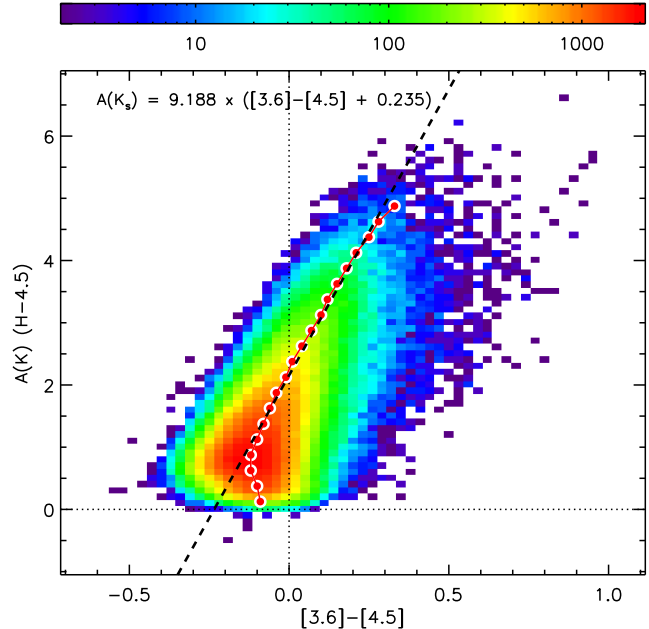


FIG. 2.— Linear fitting of $E(H - [4.5\mu])$ -derived $A(K_s)$ values as a function of $([3.6\mu] - [4.5\mu])$ color for all stars with photometric errors in the H, $[3.6\mu]$, $[4.5\mu]$ bands less than 0.07 mag . The values were binned in bins of 0.25 mag in $A(K_s)$ (red dots) and the robust linear-fit performed with the binned values. The best-fit line is shown in black.

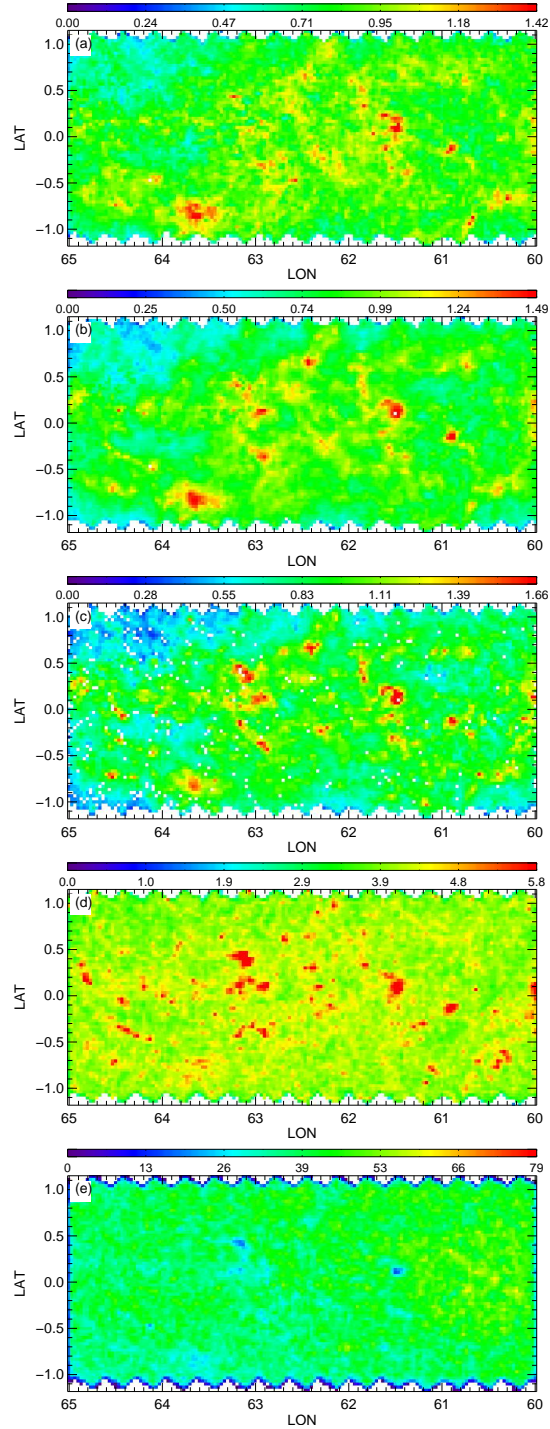


FIG. 3.— A subset of the publicly available maps. The first three maps are 90th percentile $A(K_s)$ extinction maps as derived with the RJCE method using $(H - [4.5\mu])$ colors and (a) MSTO, (b) RC, and (c) RGB stars. Panel (d) shows the 90th percentile $A(K_s)$ extinction map derived using $[3.6\mu] - [4.5\mu]$ colors of all stars (note the different colorscale ranges compared to panels a–c). Finally, panel (e) shows the starcounts map of all stars. The GLIMPSE-I data cover $10.0 < l < 65.4^\circ$ and $295.0 < l < 350.3^\circ$ and $-1 < b < +1^\circ$, while the Vela-Carina data cover $255.3 < l < 295.0^\circ$ and $-1.5 < b < +0.5^\circ$. Pixels with no stars are shown as white in the extinction maps and black in the starcounts map.

TABLE 1
MAPS IN DOWNLOADABLE FITS FILES

HDU ^a	Pop. Type	Map Type ^b	Statistic
1	MSTO	RJCE ($H - [4.5\mu]$) Extinction	Median
2	MSTO	RJCE ($H - [4.5\mu]$) Extinction	90th percentile
3	MSTO	RJCE ($H - [4.5\mu]$) Extinction	Dispersion ^c
4	MSTO	Starcounts	...
5	RC	RJCE ($H - [4.5\mu]$) Extinction	Median
6	RC	RJCE ($H - [4.5\mu]$) Extinction	90th percentile
7	RC	RJCE ($H - [4.5\mu]$) Extinction	Dispersion
8	RC	Starcounts	...
9	RGB	RJCE ($H - [4.5\mu]$) Extinction	Median
10	RGB	RJCE ($H - [4.5\mu]$) Extinction	90th percentile
11	RGB	RJCE ($H - [4.5\mu]$) Extinction	Dispersion
12	RGB	Starcounts	...
13	ALL	RJCE ($H - [4.5\mu]$) Extinction	Median
14	ALL	RJCE ($H - [4.5\mu]$) Extinction	90th percentile
15	ALL	RJCE ($H - [4.5\mu]$) Extinction	Dispersion
16	ALL	Starcounts	...
17	ALL	RJCE $[3.6\mu] - [4.5\mu]$ Extinction	Median
18	ALL	RJCE $[3.6\mu] - [4.5\mu]$ Extinction	90th percentile

¹ Extension in the FITS file.

² All extinction maps are in magnitudes of $A(K_s)$.

³ Not to be confused with an uncertainty estimate.

We note that due to the lower density of stars in the outer Galaxy data, there are a larger number of “empty” pixels in the RGB extinction maps in these directions than in the more populated inner Galaxy (although the RC and MS extinction maps suffer much less from this deficiency). Therefore, the RGB maps at these longitudes should be used with caution. Fortunately, our estimates of the distance range covered by the RC maps (Section 4.2) suggest that in these sparser outer Galaxy regions, the farthest RC stars are very likely to probe extinction to the edge of the Galactic disk; thus, the 90th percentile $A(K_s)$ RC maps may be used in place of the RGB maps where the latter are unhelpfully incomplete.

3.1. Three Dimensional Information

The derived extinction maps provide coarse *three-dimensional* information on the intrinsic interstellar dust distribution. Because each of the three stellar subsamples probes different distance ranges (see Section 4.2), comparison of the maps for a given section of sky reveals information about the distance, as well as the thickness, of individual clouds. The $l=50\text{--}60^\circ$ panels of Figure 3 demonstrate this capability. For example, the $\sim 0.5^\circ$ wide cloud centered near $(l, b) \sim (54.8^\circ, 0.8^\circ)$ in the RGB map (Figure 3c) appears in neither the MS nor the RC map, which indicates that it is a distant feature, lying beyond the reach of the RC stellar sample (~ 8 kpc; Section 4.2) but in front of the RGB sample. Similarly, the filamentary structure near $(l, b) \sim (59.0^\circ, 0.5^\circ)$ is visible in the RC and RGB maps but not the MS one, which suggests it is closer than the former cloud. An even closer structure lies at $(l, b) \sim (53.7^\circ, 0.5^\circ)$, as evidenced by the fact that it appears in the relatively short-range MS map as well as the more distant ones. In future work, we will be able to refine these cloud distance measurements after more careful calculation of the stellar distance distribution.

3.2. Uncertainty Estimates

Factors contributing to the uncertainty of RJCE extinction measurements are discussed extensively in Paper I. In summary, the uncertainty sources of (1) intrinsic scatter in the stellar colors, (2) observed photometric uncertainties, and (3) uncertainty and variation in the extinction law combine to yield a typical *individual* stellar extinction uncertainty of $\lesssim 0.11$ mag in K_s . The use of median and 90th percentile statistics in the maps further reduce the extinction uncertainty per pixel, as described in, e.g., Lombardi & Alves (2001) and Dobashi et al. (2009).

4. CAVEATS TO USAGE OF THE MAPS

4.1. Limited Photometry in Highly Reddened Regions

Apparent in many of the extinction maps in Figure 3 are sharp “holes,” generally at the higher-latitude edges of outer disk fields or at the center of high-extinction regions. The former are mostly due to an intrinsic lower stellar density (i.e., a true lack of stars) and could be remedied by reducing the map resolution; currently, for simplicity, we mask these pixels as white (see Section 3).

The holes at high extinction, however, are artifacts due to photometric limits in the adopted catalogs (here, the 2MASS PSC and GLIMPSE/Vela-Carina; see Paper I for discussion of the merged catalog limits), where a

particularly dense cloud has a total extinction sufficient to increase the magnitude of background stars beyond the limit of the catalog. When this cloud is relatively nearby, the result is an almost total lack of stars with which to measure the extinction; when the cloud is farther away, the measured extinction in the affected pixels is dominated by less-reddened foreground stars, so that the $A(K_s)$ value of the central extinction “peak” is reported to be smaller than in the rest of the cloud.

Automatically identifying which “holes” are due to which cause(s) is a nontrivial task. For the purposes of mapping extinction, there are three approaches to dealing with the second problem (i.e., artificially low $A(K_s)$ values due to the presence of a nearby dense cloud): (1) acquire deeper photometry, (2) ignore (identify and flag) the data in such pixels, or (3) use photometric bands with even lower dust sensitivity in an attempt to “see” beyond the cloud. Option (1) will become increasingly feasible as large ongoing and future IR surveys release their data, but until then, deeper IR photometry is limited to much smaller patches of sky (mostly targeted at dark clouds or the central Galactic regions), not amenable to large-scale or diffuse extinction mapping. We have chosen option (2) for the extinction maps presented here, but we enable option (3) by including $([3.6\mu] - [4.5\mu])$ extinction maps for possible use in high extinction regions.

Our analysis of catalog magnitude limits in Paper I suggests that the use of MIR data alone (i.e., not requiring a JHK_s detection) holds great promise for detecting stars behind extremely dense clouds. The extinction at $3.6\mu\text{m}$ and $4.5\mu\text{m}$ is only $\sim 0.04 \times A(V)$ (Indebetouw et al. 2005, Zasowski et al. 2009), compared to $\sim 0.2 \times A(V)$ for the H band (Cardelli et al. 1989). Figure 4 demonstrates that by using IRAC’s $[3.6\mu]$ and $[4.5\mu]$ bands alone one can trace not only the extinction peaks appearing as “holes” in the primary RJCE ($H - [4.5\mu]$) map but also an overall higher level of extinction. This is because these redder MIR bands are less susceptible to dust reddening than the NIR bands and so probe farther, while detections in JHK_s , the lack of which is the dominant cause for highly-reddened stars to be extinguished out of the band-merged 2MASS+*Spitzer* catalog, are not required. However, as discussed in greater depth in Paper I, a number of factors — including the greater intrinsic scatter in $([3.6\mu] - [4.5\mu])_0$, the increased photometric uncertainties at longer wavelengths, and the inability to distinguish stellar type (and hence identify the most distant extinction probes) because all stars have essentially the same $([3.6\mu] - [4.5\mu])$ color — render IRAC-only colors less suited for producing dereddened NIR CMDs or three-dimensional dust maps. Nevertheless, in our publicly-available maps (Section 3), we include those derived using $E([3.6\mu] - [4.5\mu])$ as an option for users interested in estimates of the *total* line-of-sight extinction.

4.2. Distance Limits

Obviously, the catalog magnitude limits discussed above (Section 4.1) translate to distance limits in the maps and define the typical depth to which each map probes. Characterization of these limits is crucial to understanding how to interpret the extinction data contained in the maps. This characterization was done in two ways.

First, we analyzed the drop in stellar density at the

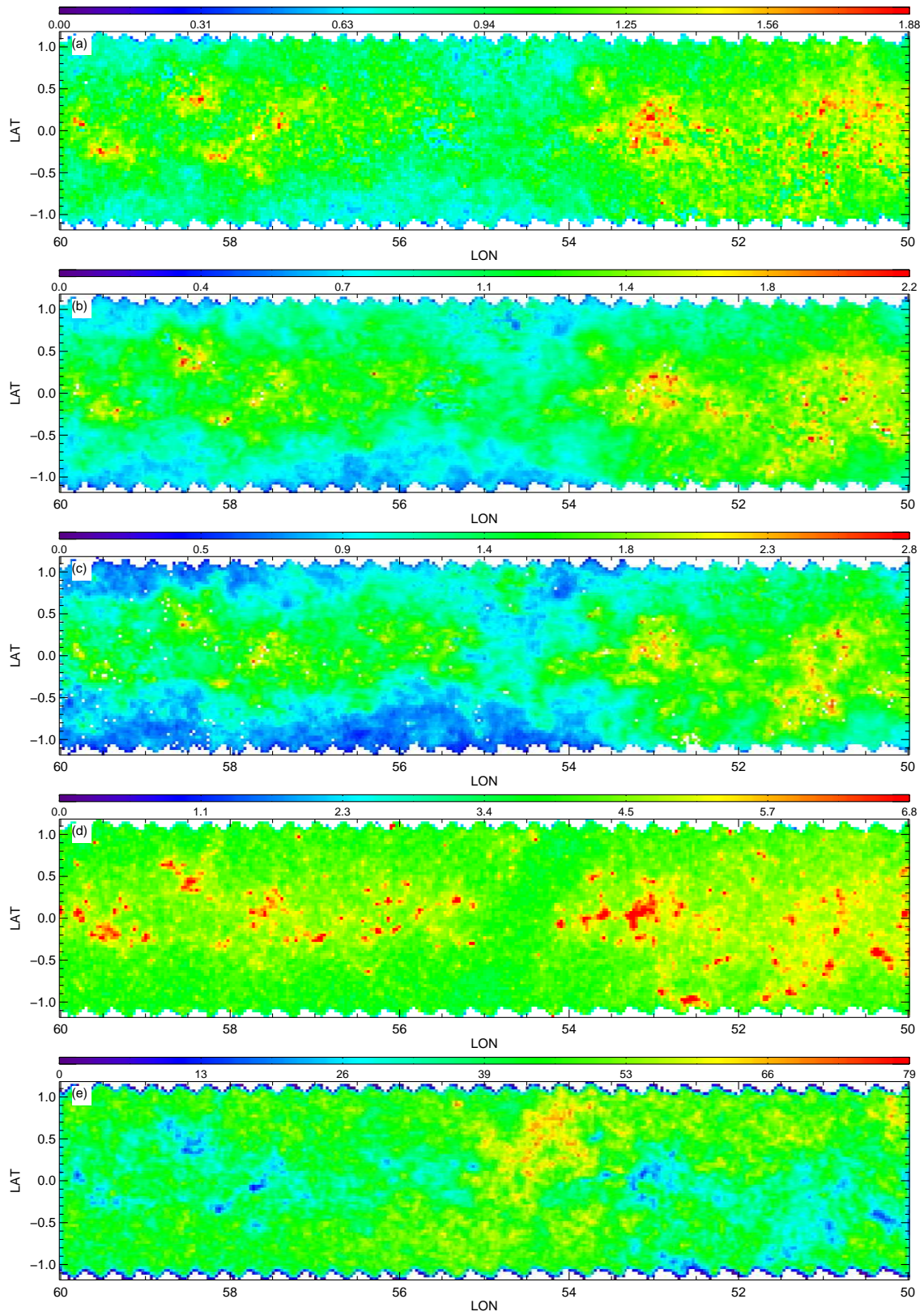


FIG. 3.— (cont.)

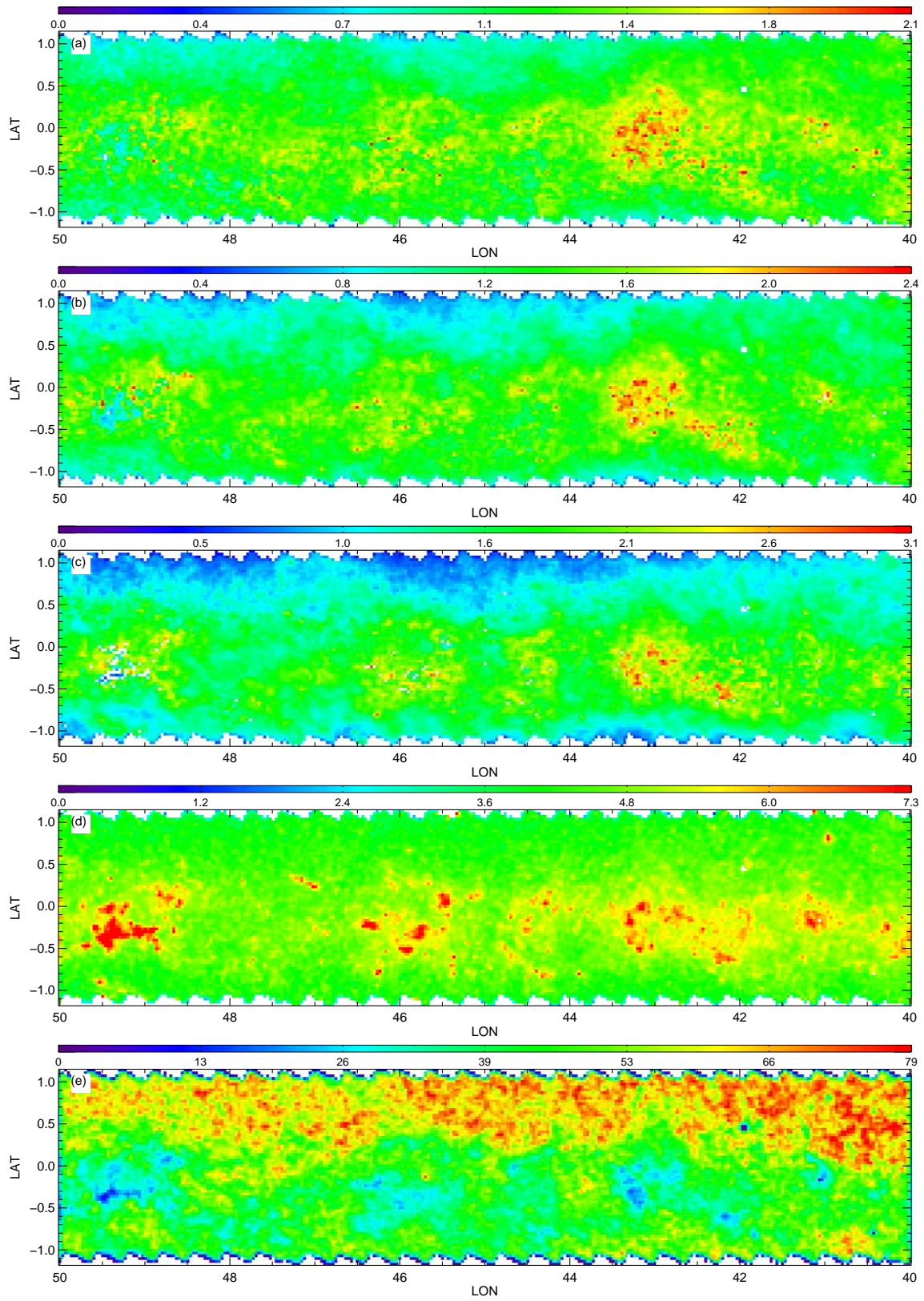


FIG. 3.— (cont.)

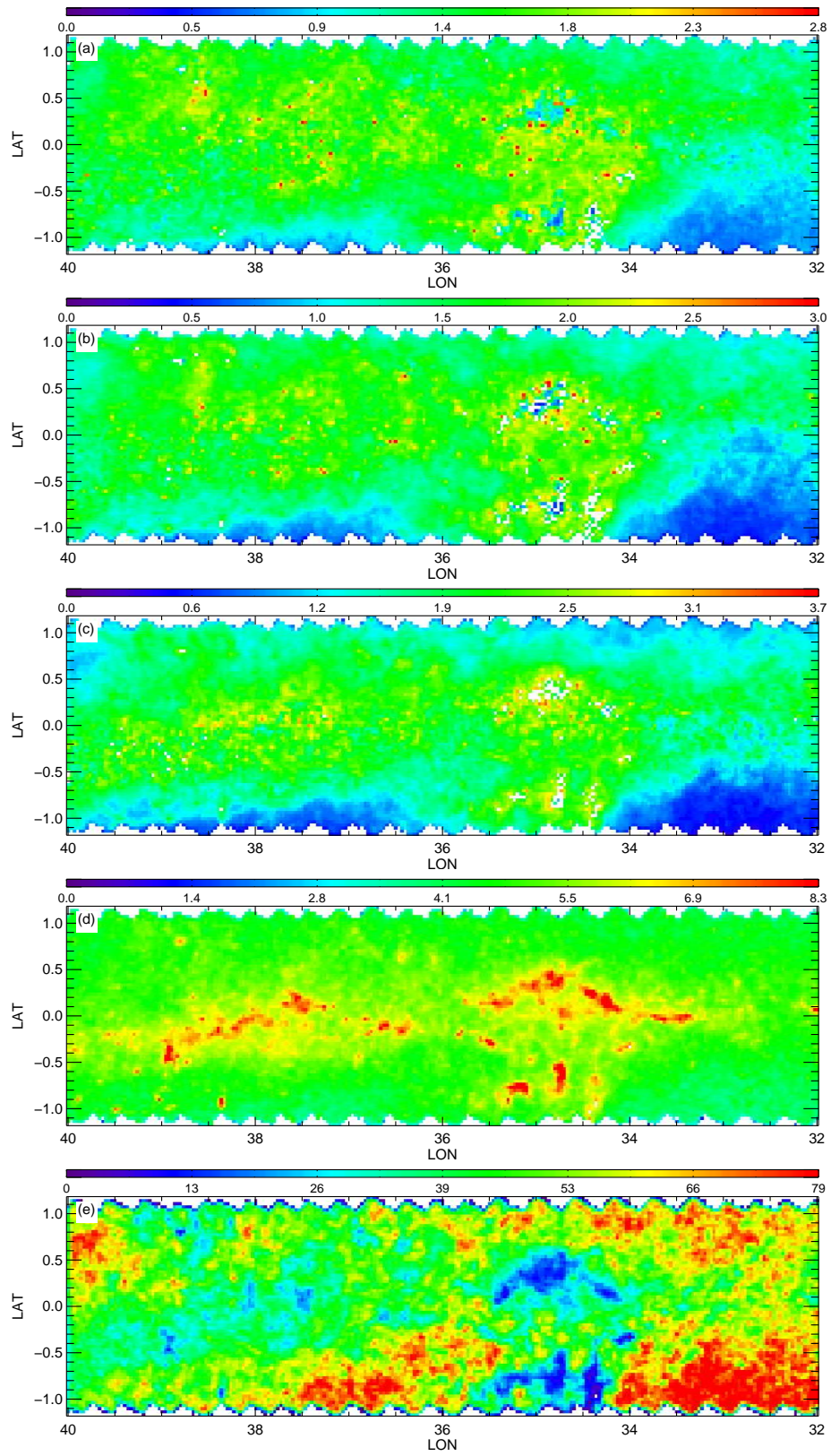


FIG. 3.— (cont.)

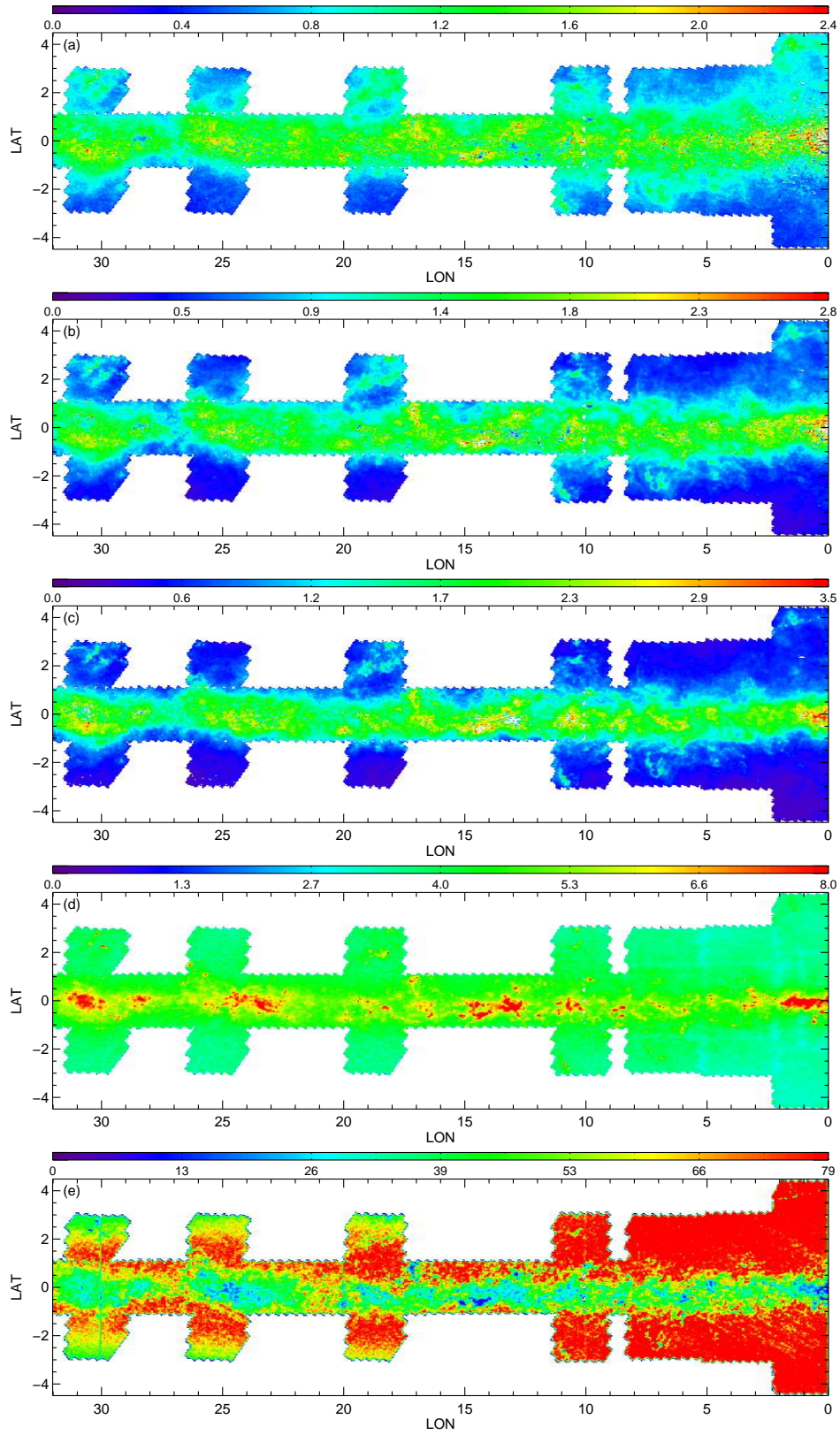


FIG. 3.— (cont.)

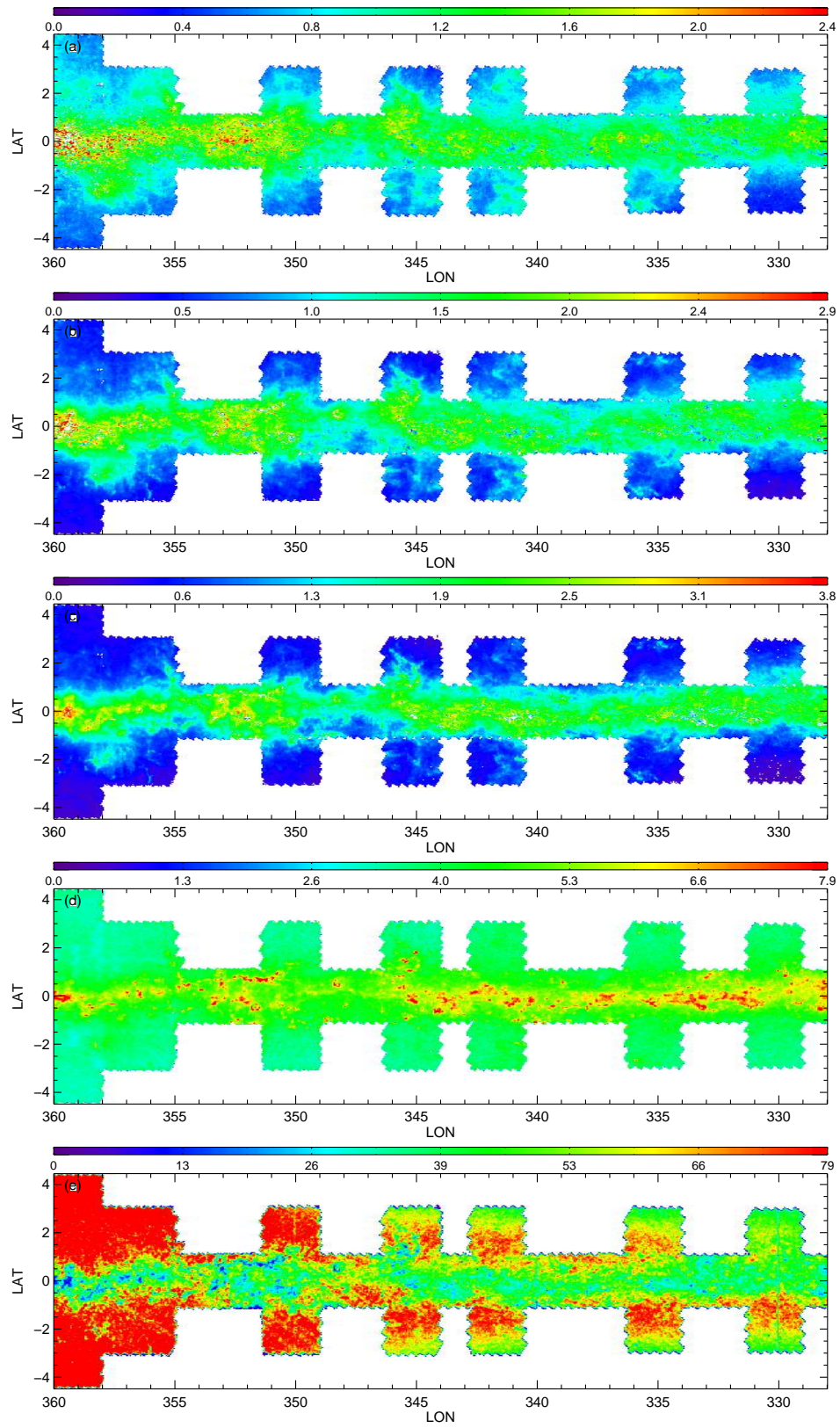


FIG. 3.— (cont.)

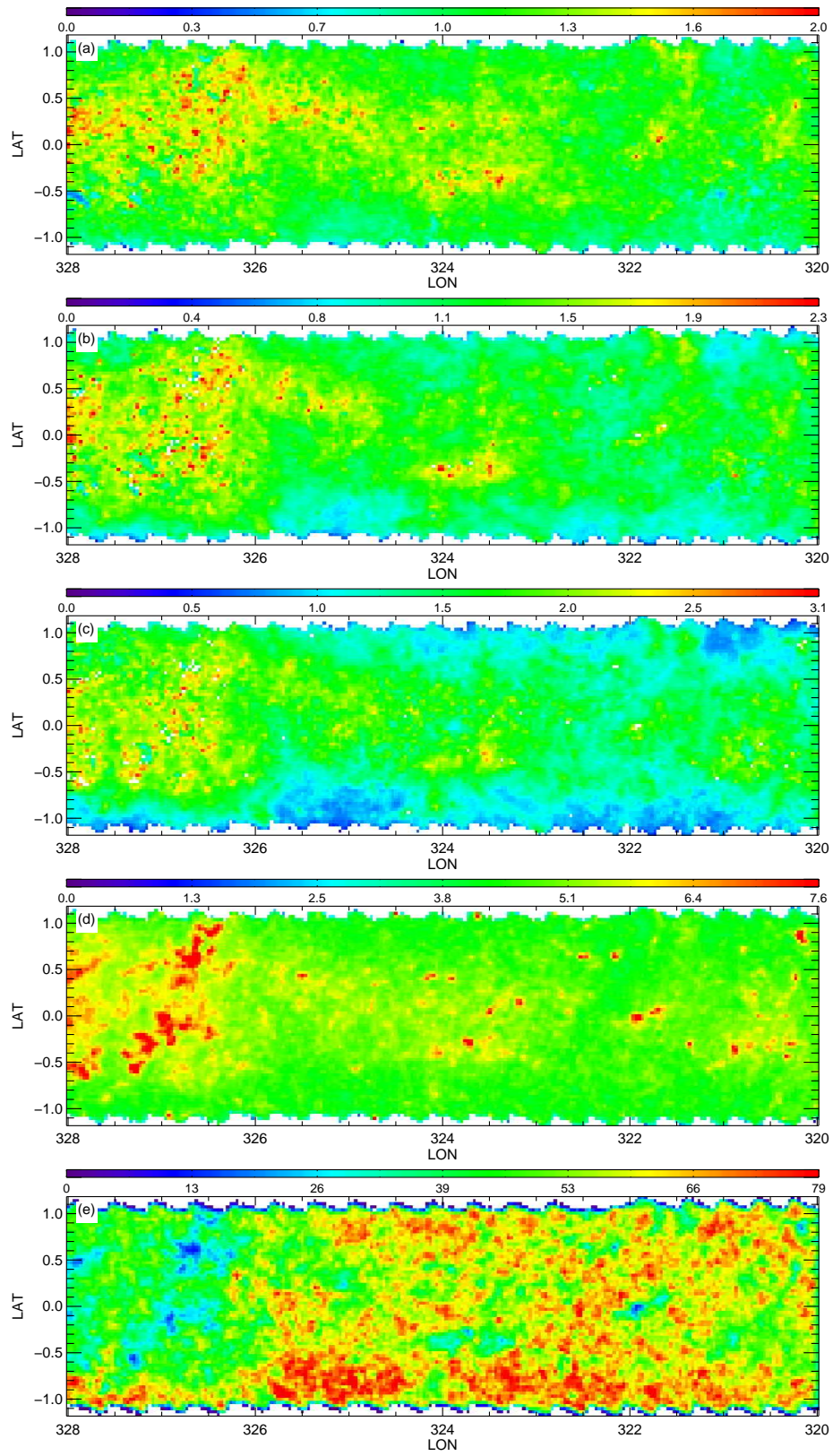


FIG. 3.— (cont.)

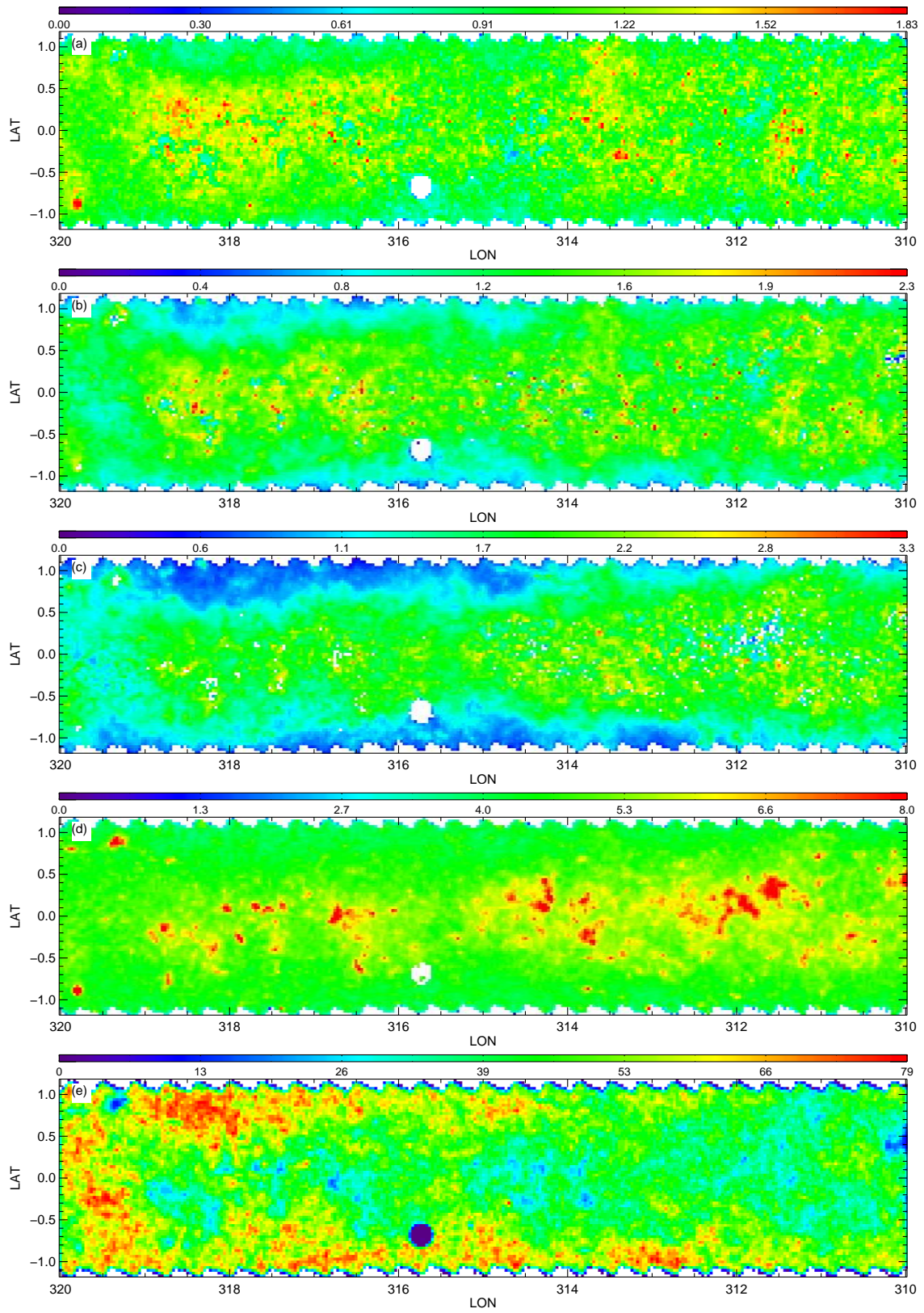


FIG. 3.— (cont.)

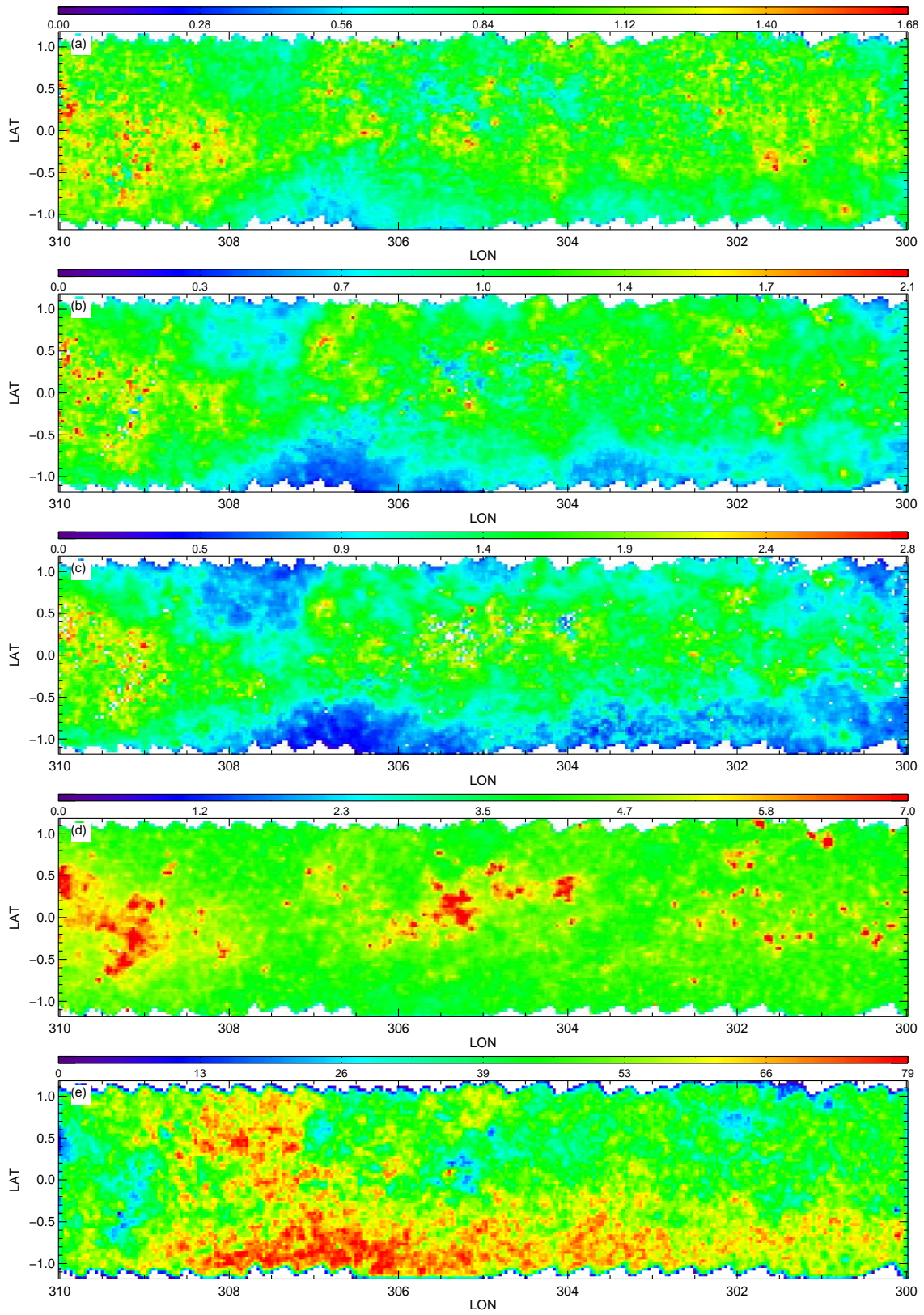


FIG. 3.— (cont.)

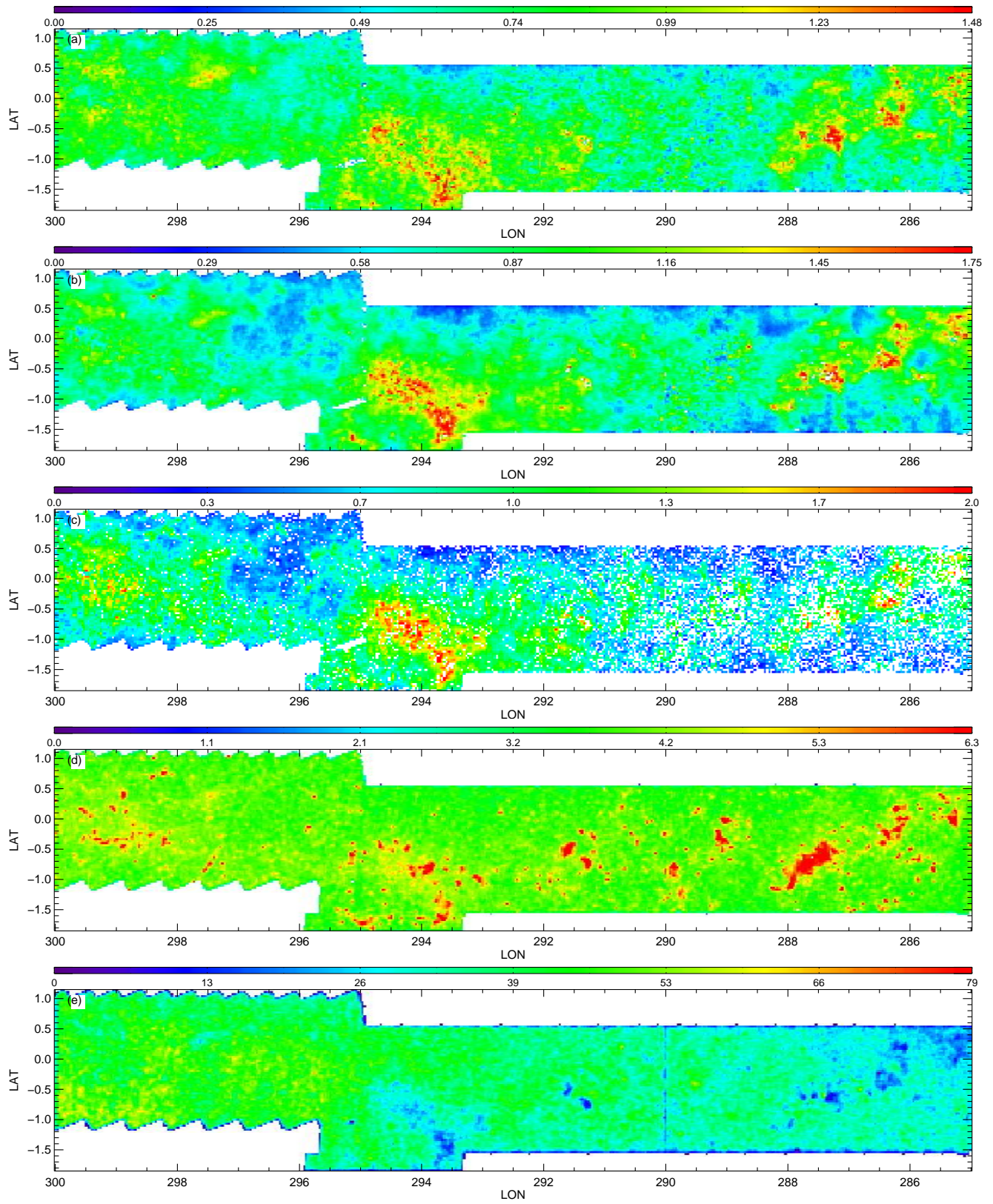


FIG. 3.— (cont.)

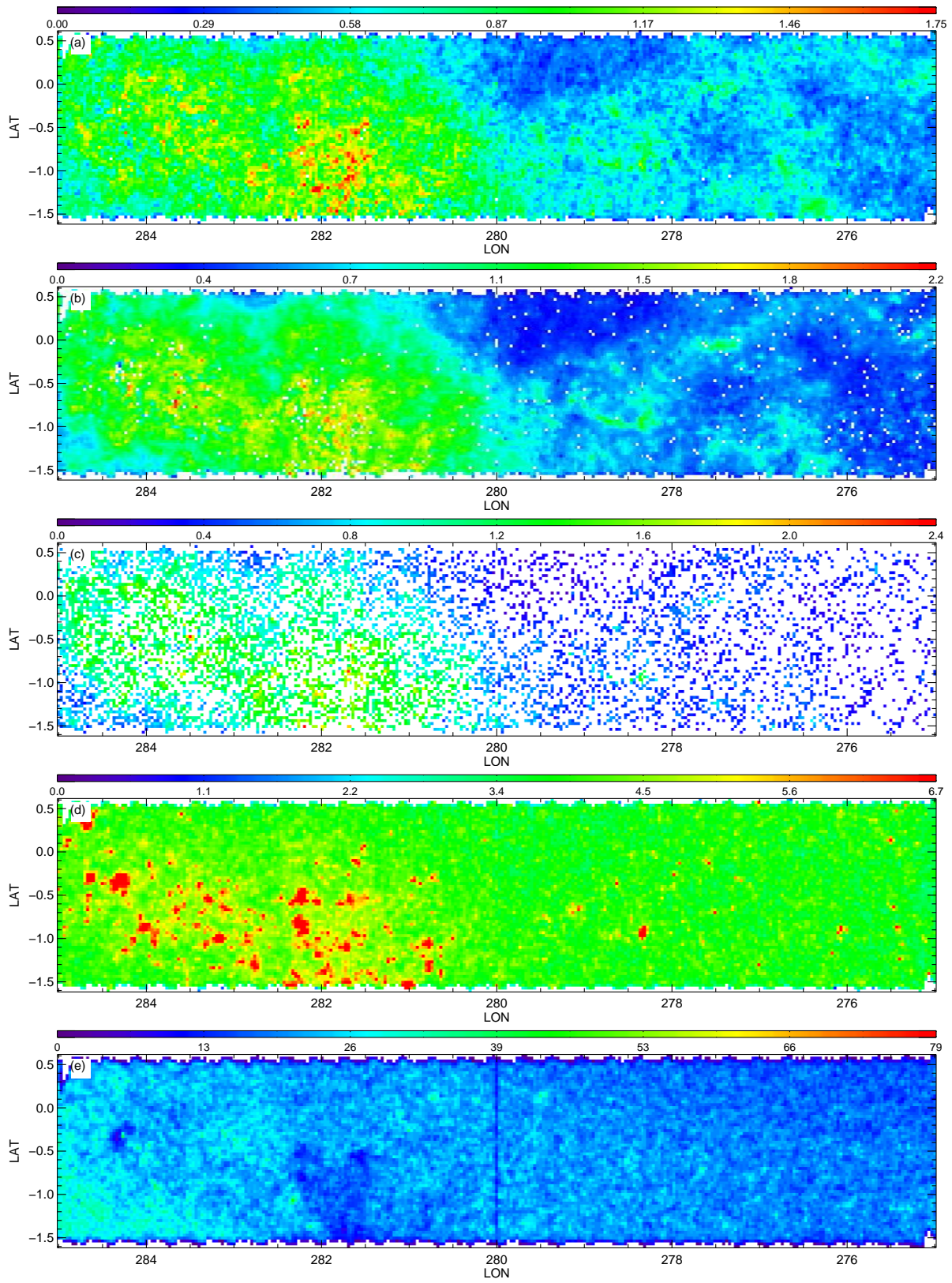


FIG. 3.— (cont.)

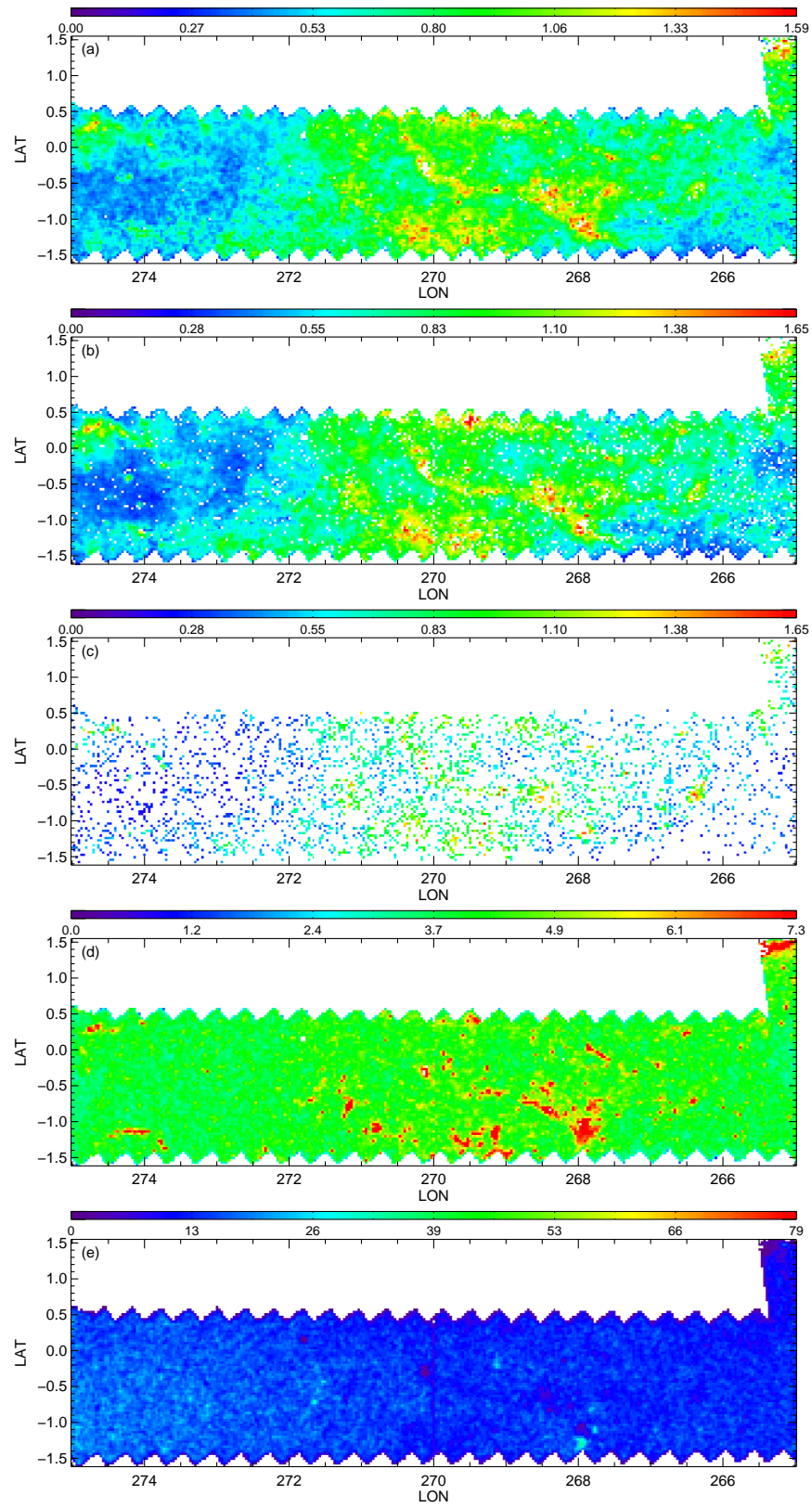


FIG. 3.— (cont.)

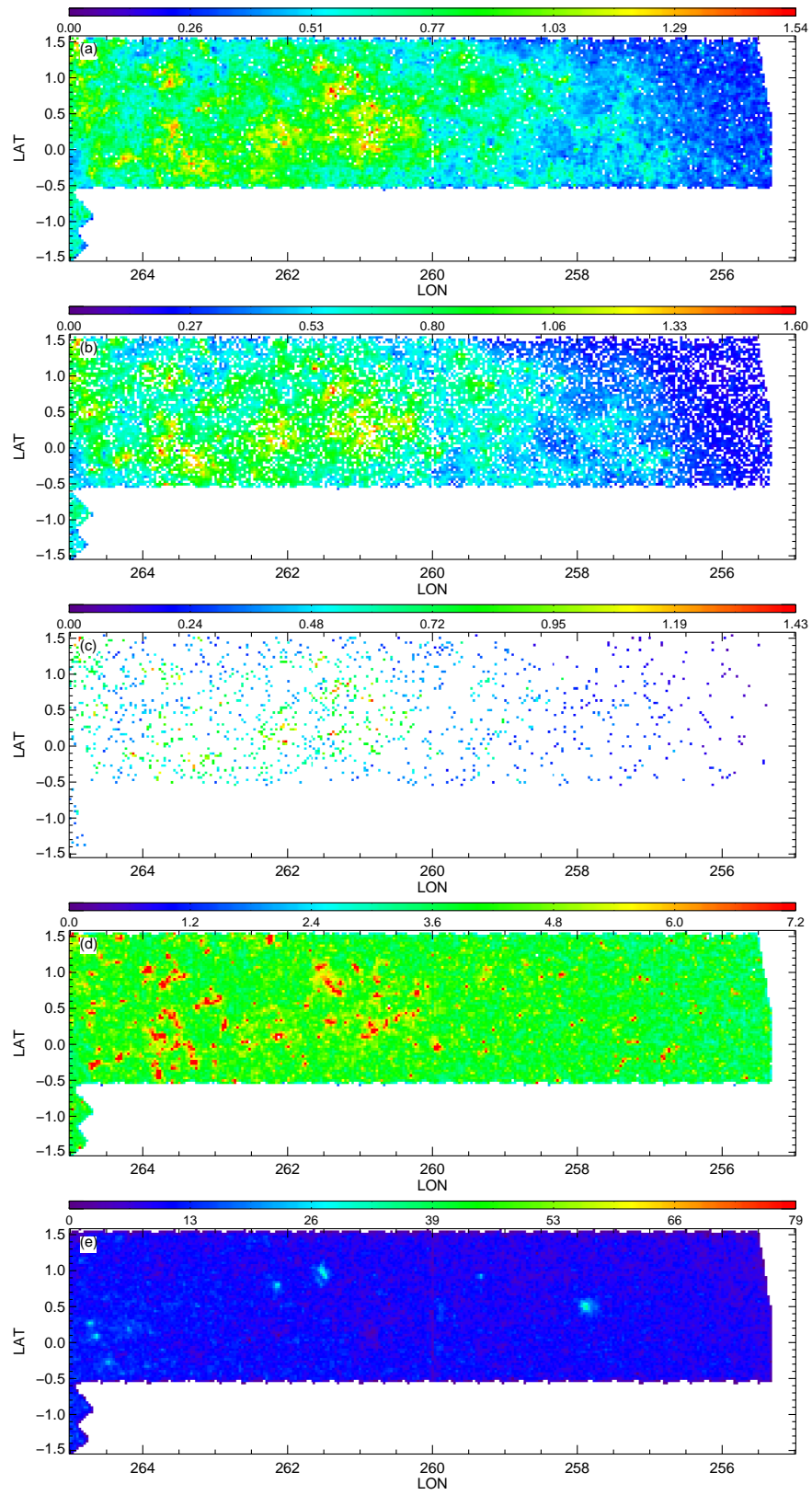


FIG. 3.— (cont.)

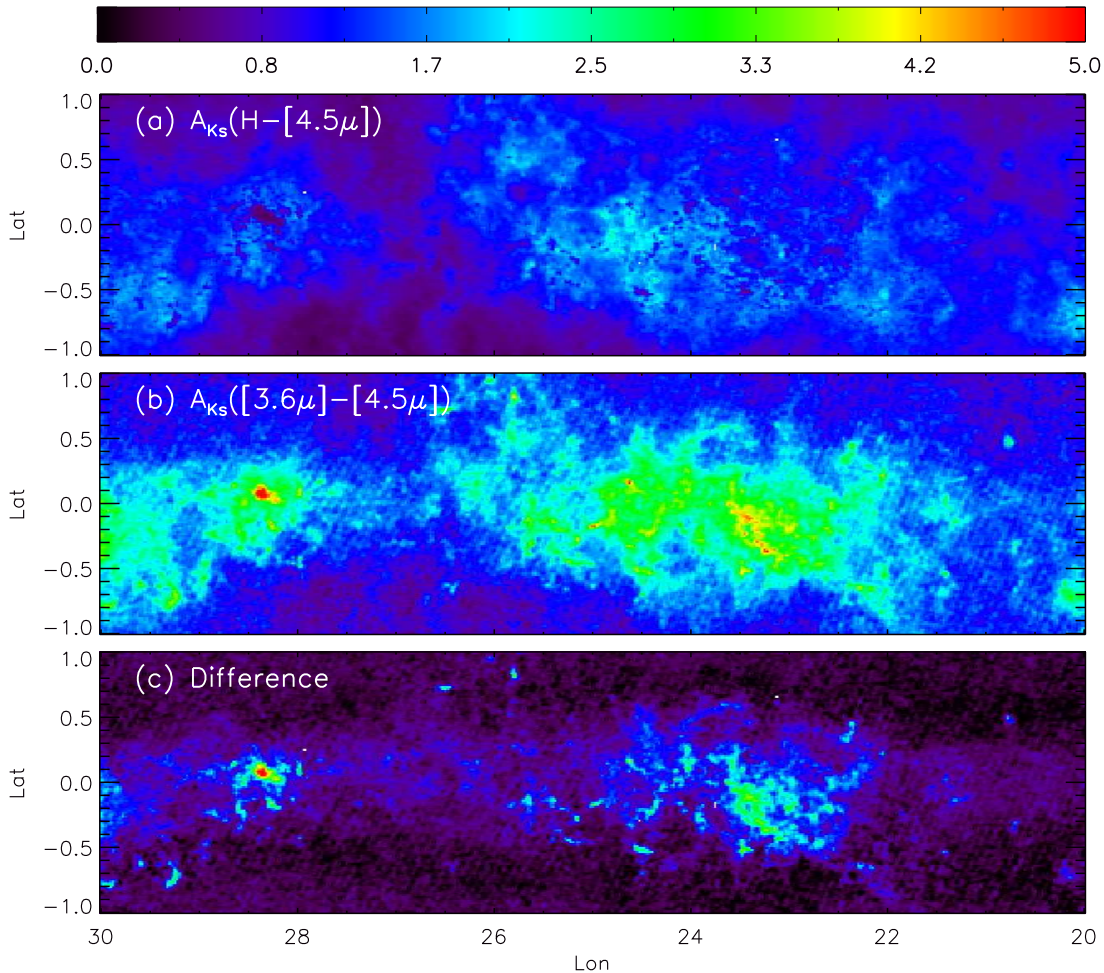


FIG. 4.— Total extinction maps (in units of $A(K_s)$ mags) made by the RJCE method, but with use of the (a) $(H - [4.5\mu])$ colors and (b) $([3.6\mu] - [4.5\mu])$ colors as the selective extinction measure (where we have adopted $([3.6\mu] - [4.5\mu])_0 = -0.1$ as a baseline color). In both cases, the stars used are those satisfying a 0.5 mag photometric uncertainty limit in only the two filters used in the color-excess measurement. Panel (c) shows the difference between the maps in panels (a) and (b). The few white pixels indicate bins containing < 2 stars.

faint edge of the RGB in dereddened CMDs throughout the GLIMPSE and Vela-Carina survey coverage. In summary, we compared the faint edge of the RGB to a suite of stellar isochrones spanning $-1.3 \leq [\text{Fe}/\text{H}] \leq +1.7$ dex and $9.0 \leq \log(\text{Age}) \leq 10.05$ yrs (Girardi et al. 2002), leaving distance as a free parameter. This provided us with a rough estimate of the distance of the farthest stars in each CMD, as well as an estimate of how likely those stars were to be at the magnitude limit of the catalog (as opposed to representing a genuine drop in stellar density, such as at the edge of the Galactic disk). The procedure used here is very similar to the one described in Paper I with the main difference that the disk edge (at a given color bin) was determined by finding the magnitude for which 90 percent of all stars in that bin are brighter. This updated method was found to produce reliable fits to the faint edge of the RGB and the results are presented in Figure 5. The filled red circles indicate the derived Galactic positions for the most distant stars in the $\Delta l = 2^\circ$ wide fields that were fit reasonably well with isochrones. Figure 5 and our comparison of the CMDs to the catalog magnitude limits are consistent in suggesting that our extinction maps from the most distant tracers (i.e., those made using the mean and 90th percentile of

RGB extinction; see Section 3) likely measure the true total Galactic extinction.

- *MSTO*: We selected all TRILEGAL model stars in a test field at $(l, b) = (30^\circ, 0^\circ)$ in the CMD region $0.0 < (J - K_s)_0 < 0.4$ and $12.5 < K_{s,0} < 13.5$, where a “clump” of MSTO stars is seen at these Galactic coordinates. The median distance of these simulated stars is ~ 2 kpc and the 90th percentile is ~ 4 kpc. Therefore, the MSTO distances are roughly 2–4 kpc.
- *RC*: Because red clump stars are standard candles (almost independent of $[\text{Fe}/\text{H}]$; Salaris & Girardi 2002) and their absolute magnitude is known fairly accurately ($M_{K_s} = -1.54 \pm 0.04$; Groenewegen 2008), we were able to calculate distances directly for our RC sample at all longitudes. Stars in the RC color range $(0.55 < (J - K_s)_0 < 0.85)$ were selected and binned in $3'$ pixels. Then, for each pixel, the RC star with the 90th percentile extinction was selected and its distance was calculated using its dereddened K_s magnitude and $M_{K_s} = -1.54$. Finally, the median distance was calculated in longitude bins of 2° ; these are shown as a solid, jagged,

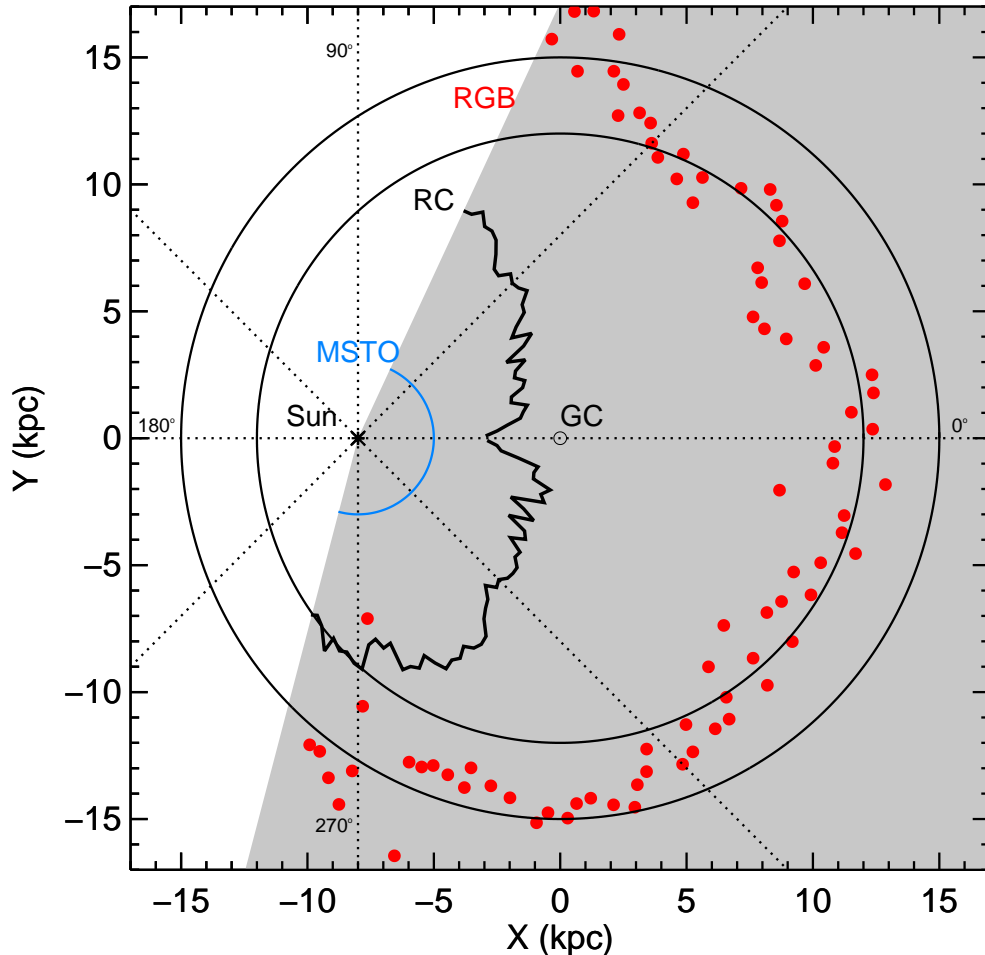


FIG. 5.— Distances of the stellar tracer populations used for the extinction maps as a function of Galactic longitude. Red filled circles indicate the maximum distance probed by the red giant branch as determined from isochrone fits to the lower edge of the dereddened RGB (§4.2). Median RC distances (in 2° bins) are shown by the black line, while the typical main sequence distance of ~ 3 kpc is shown in blue. The solid circles indicate Galactocentric radii of 12 and 15 kpc. The shaded region indicates the longitude range covered by our extinction maps.

black line in Figure 5. These distances are roughly 6–10 kpc with an average distance of 8.4 kpc.

- **RGB:** Both a TRILEGAL model and isochrones were used to estimate the RGB distances in a test field at $(l, b) = (30^\circ, 0^\circ)$. Sources with $0.85 < (J - K_s)_0 < 1.4$ and $K_{s,0} < 13.5$ were selected from the TRILEGAL model as RGB stars (only four red dwarfs contaminated this sample). The median distance for these sources is ~ 15 kpc and the 90th percentile is ~ 19 kpc. In addition, a 5 Gyr, solar metallicity Padova isochrone was used to obtain distances for observed stars with $29^\circ < l < 31^\circ$, $-1^\circ < b < +1^\circ$ and RGB colors of $0.85 < (J - K_s)_0 < 1.25$ (since the isochrone terminates at 1.25). Distances were derived assuming these were RGB stars. The median isochrone distance is ~ 10 kpc, the 90th percentile distance is ~ 24 kpc, and the median value in a 90th percentile binned distance map (with $3'$ pixels) is 22.9 kpc. In comparison, the “CMD edge” distances described

above are on average 15 kpc. Therefore, the RGB distances are roughly 15–24 kpc.

- **ALL:** Since the vast majority of the stars in the data set are red clump stars, the distance limits for maps that make use of all stars are likely to be similar to the limits for RC stars.

The reader is referred to Figure 5, which shows distances of the stellar tracers. The RGB maps probe to the edge of the Galactic disk and can be considered close to “total line-of-sight extinction” maps in nearly all directions covered by the maps.

5. PUBLIC ACCESS TO THE MAPS

To encourage usage, additional comparisons, and feedback from the astronomical community, we have made public 515 deg^2 of midplane and bulge extinction maps using the RJCE method outlined in Paper I and the present paper — i.e., using the $(H - [4.5\mu])$ color with H -band photometry from 2MASS and $[4.5\mu]$ data from

Spitzer-IRAC. In addition, we provide $E([3.6\mu] - [4.5\mu])$ -derived extinction maps for “all stars” which are useful in heavily-extincted regions, and 2MASS starcount maps that are roughly anti-correlated with extinction. The regions included in this public release are those covered by the GLIMPSE-I, -II, -3D, and Vela-Carina surveys, spanning $255.3 \leq l \leq 65.4^\circ$ and, in general, for $|b| \leq 1^\circ - 1.5^\circ$ (the Vela-Carina data is centered slightly off the midplane to track the highest extinction regions) but up to $b \sim 4^\circ$ for certain longitudes (for GLIMPSE-II and -3D). These maps are available at <http://www.astro.virginia.edu/rjce/> as quick-look GIF images and downloadable FITS files along with querying software written in IDL.

Included on the website are instructions for the download and use of the maps and software, as well as notes regarding the known caveats. We welcome any feedback from the community that may help improve these tools, and we plan to post refined and improved maps as our methodology evolves.

6. SUMMARY AND FUTURE WORK

We have developed a method for measuring line-of-sight extinction that combines near- and mid-infrared photometry (from 2MASS + *Spitzer*-IRAC) to calculate stellar reddening in a process that is (i) robust to variations in intrinsic stellar type and (ii) recovers the intrinsic stellar type. This Rayleigh-Jeans Color Excess (RJCE) technique represents a major improvement on previous color-excess measurements because it includes reddening corrections of temperature-sensitive near-infrared colors which allows us to create dereddened CMDs (extremely useful for stellar population studies) and select reasonably pure samples of stars of specific stellar type or luminosity class. In Paper I of this series, we described the RJCE method in great detail. This installment presents a large, publicly-available atlas of two-dimensional, high angular resolution extinction maps created from RJCE-derived extinction values.

We take advantage of RJCE’s ability to discriminate stellar spectral type to produce extinction maps generated independently from three groups of stars dominated by distinct stellar populations (main sequence [MS] dwarfs, red clump [RC] giants, and red giant branch [RGB] stars), each of which probes different heliocentric distance ranges and thus traces the net dust column to different distances. Comparison of these maps for any given section of the Galactic midplane provides rough *three-dimensional* information on the intrinsic dust distribution and allows clouds and cloud complexes to be isolated to specific distance ranges. We present a total of ten different types of extinction maps (in units of $A(K_s)$), each encompassing $\sim 515 \text{ deg}^2$ of the dustiest regions of the Galactic midplane, using data from the 2MASS-PSC merged with *Spitzer*-IRAC photometry from the GLIMPSE-I/-II/-3D and Vela-Carina surveys. For each of the three stellar tracer subsamples (MS, RC, and RGB) and “all stars”, we provide maps giving two different statistical estimates of the $(H - [4.5\mu])$ -derived extinction: the median and 90th percentile $A(K_s)$ in each spatial pixel. The three 90th percentile maps probably provide the most reliable estimate of the total integrated extinction affecting each subsample population to the maximum distance probed. Additionally, we provide

median and 90th percentile $([3.6\mu] - [4.5\mu])$ -derived extinction maps of “all stars”, which provide reasonable extinction estimates for very dusty regions where the other maps fail due to lack of stars.

Section 4 provides caveats to the applicability of our maps as well as distance limits for the different tracer populations. We find that our RGB 90th percentile maps very likely represent the total Galactic extinction in near all directions. Our 90th percentile RC maps probe to an average distance of ~ 8 kpc, while the MS maps are limited to 2–4 kpc.

The possibility of using MIR-only colors to estimate extinction where NIR-MIR colors are unavailable (due to the increased extinction in the NIR bands or the lower resolution of 2MASS) is also explored. Though MIR-only colors do not carry enough information to allow stellar type selection (and thus reliable distance estimates), we find that they can provide extinction estimates in the most highly extinguished portions of our maps (such as cloud cores and regions near the Galactic center). Thus, we include in our public atlas extinction maps derived from MIR-only reddening to serve as strong lower limits to the total extinction; this is most useful in the inner Galaxy, where even the RGB maps from typical RJCE colors are insufficient to probe to the far edge of the Galactic disk.

An extensive program for application and improvement of the RJCE methodology is anticipated. We are working to improve the RJCE extinction estimates using a more refined treatment of stellar properties, and the ongoing APOGEE survey (Majewski et al. 2010) will allow us to compare RJCE-derived stellar types to spectroscopically-determined ones. We are evaluating the benefit of using optimized “hybrid”-color schemes (i.e., merging extinction estimated using long-baseline NIR-MIR colors and MIR-only colors) where high extinction or confusion limits the depth of the NIR photometry. Our ultimate goal is to apply this dereddening methodology to ascertain the three-dimensional distribution of both dust and stars within the Galactic midplane. We have already taken advantage of our extensive data set to characterize the wavelength dependence of IR extinction throughout the midplane (Zasowski et al. 2009), and work is under way to use the new, reliably-cleaned CMDs to explore heavily-reddened or otherwise elusive Galactic structures, such as the central bar(s) and the outer spiral arms and the edges of the disk.

We thank R. Indebetouw and M. F. Skrutskie for helpful discussions, and M. Meade and B. Babler for their efforts to reduce the Vela-Carina dataset with the GLIMPSE pipeline. We thank the anonymous referee for useful comments and suggestions. SRM appreciates the hospitality of the Observatories of the Carnegie Institution of Washington for hosting a sabbatical visit during which this project was conceived. We acknowledge support from NSF grants AST-0307851 and AST-0807845, and funding from NASA *Spitzer* grants 1276756 and 1316912. DLN has been supported by an ARCS Scholarship, a VSGC Graduate Research Fellowship, and an SDSS-III APOGEE postdoc, and GZ has been supported by a VSGC Graduate Research Fellowship, a NASA Earth & Space Science Fellowship, and a UVa

Dissertation Acceleration Fellowship. This work is based in part on observations made with the *Spitzer* Space Telescope, and has made use of the NASA / IPAC Infrared Science Archive, which are operated by the Jet Propulsion Laboratory, California Institute of Technology un-

der a contract with NASA. We acknowledge use of data products from the Two Micron All Sky Survey, a joint project of the University of Massachusetts and the Infrared Processing and Analysis Center / California Institute of Technology, funded by NASA and the NSF.

REFERENCES

- Alves, J., Lada, C. J., Lada, E. A., Kenyon, S. J., & Phelps, R. 1998, *ApJ*, 506, 292
- Amôres, E. B., & Lépine, J. R. D. 2005, *AJ*, 130, 659
- Amôres, E. B., & Lépine, J. R. D. 2007, *AJ*, 133, 1519
- Arce, H., Goodman, A. 1999a, *ApJLetters*, 512, L135
- Barnard, E. E., Frost, E. B., & Calvert, M. R. 1927, *A Photographic Atlas of Selected Regions of the Milky Way*, [Washington] Carnegie institution of Washington, 1927.,
- Benjamin, R. A., et al. 2003, *PASP*, 115, 953
- Bohlin, R. C. 1975, *ApJ*, 200, 402
- Bok, B. J. 1956, *AJ*, 61, 309
- Burstein, D., & Heiles, C. 1978, *ApJ*, 225, 40
- Burstein, D., & Heiles, C. 1982, *AJ*, 87, 1165
- Burstein, D., Bertola, F., Buson, L. M., Faber, S. M., & Lauer, T. R. 1988, *ApJ*, 328, 440
- Burstein, D. 2003, *AJ*, 126, 1849
- Cambrésy, L., Jarrett, T. H., & Beichman, C. A. 2005, *A&A*, 435, 131
- Cardelli, J., Clayton, G., Mathis, J. 1989, *ApJ*, 345, 245
- Chen, B., Figueras, F., Torra, J., Jordi, C., Luri, X., & Galadí-Enriquez, D. 1999, *A&A*, 352, 459
- Choloniewski, J., & Valentijn, E. A. 2003, *Acta Astronomica*, 53, 265
- Churchwell, E., Babler, B. L., Meade, M. R., et al. 2009, *PASP*, 121, 213
- de Vaucouleurs, G., & Buta, R. 1983, *AJ*, 88, 939
- de Vaucouleurs, G., de Vaucouleurs, A., & Corwin, J. R. 1976, *Second reference catalogue of bright galaxies*, 1976, Austin: University of Texas Press., 0
- Dobashi, K., Bernard, J.-P., Kawamura, A., et al. 2009, *AJ*, 137, 5099
- Dutra, C., Santiago, B., Bica, E., Barbuy, B. 2003a, *MNRAS*, 338, 253
- Dutra, C. M., Ahumada, A. V., Clariá, J. J., Bica, E., & Barbuy, B. 2003b, *A&A*, 408, 287
- Fabbri, R., Guidi, I., Natale, V., & Ventura, G. 1986, *Fourth Marcel Grossmann Meeting on General Relativity*, 789
- Faber, S. M., Wegner, G., Burstein, D., Davies, R. L., Dressler, A., Lynden-Bell, D., & Terlevich, R. J. 1989, *ApJS*, 69, 763
- Fong, R., Jones, L. R., Shanks, T., Stevenson, P. R. F., & Strong, A. W. 1987, *MNRAS*, 224, 1059
- Froebrich, D., Ray, T. P., Murphy, G. C., & Scholz, A. 2005, *A&A*, 432, L67
- Girardi, L., Groenewegen, M. A. T., Hatziminaoglou, E., & da Costa, L. 2005, *A&A*, 436, 895
- Girardi, L., et al. 2002, *A&A*, 391, 195
- Groenewegen, M. A. T. 2008, *A&A*, 488, 935
- Gosling, A. J., Bandyopadhyay, R. M., & Blundell, K. M. 2009, *MNRAS*, 394, 2247
- Heiles, C. 1976, *ApJ*, 204, 379
- Herschel, W. 1785, *Philosophical Transactions*, 75, 213
- Hilditch, R. W., Hill, G., & Barnes, J. V. 1983, *MNRAS*, 204, 241
- Holmberg, E. B. 1974, *A&A*, 35, 121
- Indebetouw, R., et al. 2005, *ApJ*, 619, 931
- Ivans, I. I., Sneden, C., Kraft, R. P., Suntzeff, N. B., Smith, V. V., Langer, G. E., & Fulbright, J. P. 1999, *AJ*, 118, 1273
- Jenkins, E. B., & Savage, B. D. 1974, *ApJ*, 187, 243
- Jones, T. J., Hyland, A. R., & Bailey, J. 1984, *ApJ*, 282, 675
- Jones, T. J., Hyland, A. R., Robinson, G., Smith, R., & Thomas, J. 1980, *ApJ*, 242, 132
- Knapp, G. R., & Kerr, F. J. 1974, *A&A*, 35, 361
- Knude, J. 1996, *A&A*, 306, 108
- Kron, G. E., & Guetter, H. H. 1973, *PASP*, 85, 534
- Lada, C. J., Lada, E. A., Clemens, D. P., & Bally, J. 1994, *ApJ*, 429, 694
- Lada, C. J., Lombardi, M., & Alves, J. F. 2009, *ApJ*, 703, 52
- Lilley, A. E. 1955, *ApJ*, 121, 559
- Lombardi, M., & Alves, J. 2001, *A&A*, 377, 1023
- Lombardi, M. 2009, *A&A*, 493, 735
- Lombardi, M., Lada, C. J., & Alves, J. 2010, *A&A*, 512, A67
- Lucas, P. W., et al. 2008, *MNRAS*, 391, 136
- Majewski, S. R., Wilson, J. C., Hearty, F., Schiavon, R. R., & Skrutskie, M. F. 2010, *IAU Symposium*, 265, 480
- Majewski, S., Babler, B., Churchwell, E., et al. 2007, *Spitzer Proposal ID #40791*, 40791
- Majewski, S. R., Zasowski, G., & Nidever, D. L. 2011, *ApJ*, 739, 25
- Noonan, T. W. 1971, *AJ*, 76, 190
- Peek, J. E. G., & Graves, G. J. 2010, *ApJ*, 719, 415
- Peterson, B. A. 1970, *AJ*, 75, 695
- Rocha-Pinto, H. J., Majewski, S. R., Skrutskie, M. F., Crane, J. D., & Patterson, R. J. 2004, *ApJ*, 615, 732
- Salaris, M., Girardi, L. 2002, *MNRAS*, 337, 332
- Sandage, A. 1973, *ApJ*, 183, 711
- Savage, B. D., & Jenkins, E. B. 1972, *ApJ*, 172, 491
- Savage, B. D., Bohlin, R. C., Drake, J. F., & Budich, W. 1977, *ApJ*, 216, 291
- Schlegel, D., Finkbeiner, D., Davis, M. 1998, *ApJ*, 500, 525 (SFD)
- Seki, M. 1973, *A&A*, 28, 207
- Skrutskie, M. F., et al. 2006, *AJ*, 131, 1163
- Smith, R. G. 1987, *MNRAS*, 227, 943
- Stanek, K. Z. 1998a, *arXiv:astro-ph/9802093*
- Stanek, K. Z. 1998b, *arXiv:astro-ph/9802307*
- Struve, F. G. W. 1847, *Etudes d'astronomie stellaire sur la voie lactée et sur la distance des étoiles fixes*, (St. Petersburg: Imprimerie de L'Académie Impériale des Sciences)
- Sturch, C. 1969, *AJ*, 74, 82
- Trumpler, R. 1930, *Lick Obs. Bull.*, 14, 154
- von Braun, K., & Mateo, M. 2001, *AJ*, 121, 1522
- Wolf, M. 1923, *Astronomische Nachrichten*, 219, 109
- Yasuda, N., Fukugita, M., & Schneider, D. P. 2007, *AJ*, 134, 698
- Zasowski, G., et al. 2009, *ApJ*, 707, 510